# Understanding the Mechanics of complex topology of the 3D printed Anthill architecture

Brijesh Kushwaha[1†], Avinash Kumar[2†], Rushikesh S. Ambekar[1†*], Vinay Arya[2], Solomon Demiss Negedu[3], Deep Bakshi[4], Emmanuel Femi Olu[3], Ravi Sastri Ayyagari[4], Varinder Pal[1], Kishor Kumar Sadasivuni[5*], Nicola M. Pugno[6*], Chirodeep Bakli[2*], Chandra S. Tiwary[1*]

[1]Department of Metallurgical and Materials Engineering, Indian Institute of Technology Kharagpur, Kharagpur 721302, India

[2]School of Energy Science & Engineering, Indian Institute of Technology Kharagpur, Kharagpur 721302, India

[3]Department of Materials Science & Engineering, Jimma Institute of Technology (JIT), Jimma 378, Ethiopia

[4]Department of Mechanical Engineering, Indian Institute of Technology, Gandhinagar 382355, India

[5]Center for Advanced Materials, Qatar University, Qatar

[6]Laboratory for Bionic, Nano, Meta, Materials & Mechanics, Department of Civil, Environmental and Mechanical Engineering, University of Trento, Via Mesiano, 77, 38123 Trento, Italy

[†] Equal contribution

*Email: rambekar@iitkgp.ac.in (RSA), kishorkumars@qu.edu.qa (KKS), nicola.pugno@unitn.it (NMP), chirodeep@iitkgp.ac.in (CB) and Chandra.tiwary@metal.iitkgp.ac.in (CST)

## ABSTRACT

**Objectives:** The present work aimed to investigate the deformation behavior of complex ant mound architectures under compression.

**Methods:** We have used the cement casting method to extract four different ant nest morphologies. These casted cement structures were digitalized using a 3D micro-computer tomography (CT) scan. The digitized structures were simulated under different loading conditions using Finite Element Methods (FEM). In order to supplement the numerical

understanding, the digital architectures were 3D printed and experimentally tested under uniaxial loading conditions.

**Results:** Ants produce a variety of complex architectures for adapting to the surrounding environment and ants' needs. Ant mound consists of at least one pillar with a broad base tapered towards its tip. Anthill architectures have unique topological features. Mechanical strength of ant mould can be 600 times enhanced by tuning topology. Thickness and angle of pillars have huge effect on load-bearing property

**Conclusion:** The branched structures can endure larger stress and deform in the process under a volumetric pressure application, making them sacrificial units for extreme disasters like floods and earthquakes. The 3D printing experiments and Finite Element Methods simulations are needed to tackle the complex ant mound architectures and appear in good agreement, suggesting a robust design and thus the possibility of constructing anthill-inspired civil buildings with a tree-trunk-like geometry.

Keywords: 3D printing; Bio-inspired architecture; Ant mound; Mechanical properties; Young's modulus; Polylactic acid.

## 1. INTRODUCTION

Nature builds complex architectures that can sustain harsh environmental conditions by not only bearing high loads but also resisting permanent damage [1]. These complex architectures are often created by living species, which develop these techniques through years of evolution. The topology of these architectures is designed to handle the extremities of nature in order to survive. Their structures, textures, and arrangements are complex and robust, which attracts the attention of researchers. Beehives, spider-nets, termite-hills, sea-shell, etc., have inspired researchers to mimic their design and investigate the role of topology in the evolution of such complex architectures. For example, the complex architecture of the rigid wall of the

termite hill is made of soil glued with saliva, which inspired the building of geotechnical tools for mineral exploration [2,3]. Similarly, bees honeycomb (hexagonal) hierarchical structures [4–9] and spider webs [10] have been investigated to explore their architecture and their utilization towards the damage tolerant lightweight design. Some living organisms have shells attached to their body, for example, snails, mollusks, horseshoe crabs, and turtles, to name a few. The shells act as their home and protect them from predation and other threats. The shape and material of seashells [11], the bony and cartilaginous shell of turtles [12], and the nacre produced by some mollusks as an inner shell layer [13,14], etc. have always been attractive areas of research [15,16].

Ants build one of the most impressive and intricate nests architecture below the earth's surface [1,17]. The resulting complexity of the nest architecture emerges from a self-organized process [18–20]. These interactions determine the collective behaviors, such as a colony's speed of recruitment to food and chamber connectivity, etc. The ants' nests are built in a complex architecture containing irregular descending shafts, horizontal chambers, and tunnels [19,21,22]. These elongated voids with a circular, oval, or flattened-oval cross-section, with a long axis usually inclined from the vertical by $20^{o}$ to $70^{o}$ (rarely $90^{o}$) called shafts. They are modular units of nest growth; nests are enlarged by adding more shafts or extending the existing ones [21,23]. These unique topological features of the nest also depend on the life cycle and colony growth. Nest excavation rates and final nest sizes increased with colony size because, in the largest colonies, the internal surface area was scaled with volume [24–27]. It is known that ant nests are constructed underground such that they can bear the loads applied accidentally by other living creatures over the surface or force applied due to natural phenomena.

Most studies of ant nest architecture have focused on nest complexity, i.e., subterranean chambers, shafts nodes, and tunnels [28–30]. However, the contribution of structural morphology towards enhancing mechanical robustness of ant nest architecture has received

much less attention. Nowadays, with the advent of the 3D printing (3DP) technique, researchers started using it widely for mimicking nature-inspired structures [31–33], molecule-inspired structures [34–37], mathematical model-based structures [38,39], etc. With the help of the 3DP technique, we can realize the complex architecture of the ant nest with high accuracy, making it easily accessible, affordable, and environment friendly [40]. 3D printing techniques provide design flexibility; therefore complex structures can be easily fabricated. The design of the complex structures can be improved with a topology optimization tool which provides the best possible results by optimizing the design in the desired constrained space [41]. Topology optimization tools with 3D printing can enhance the efficiency of the applications such as structural architecture [42], robotics (soft actuators) [43,44] and the biomedical field (bone tissue engineering) [45]. Researchers are also taking advantage of hybrid machine learning tools for 3D printing process optimization [46].

In this paper, we have studied the mechanical robustness of 3D printed ant mound structures, which is not available in solitary literature. We have used the cement casting method to extract four different ant nest morphologies. These cement structures were digitalized using a 3D micro-computer tomography (CT) scan. The digitized structures were simulated under different loading conditions using Finite Element Methods (FEM). In order to supplement the numerical understanding, the digital architectures were 3D printed and experimentally tested under uniaxial loading conditions. Subsequently, a combined numerical and experimental analysis has been done to delineate the contribution of structural topology and materials to the strength and resistance to deformation of ant nest architectures, showing interesting bio-inspired solutions.

## 2. MATERIALS AND METHODS

### 2.1. DESIGN AND FABRICATION

All 3D printed structures were created in Ultimaker 3 Extended printer using Polylactic acid (PLA). PLA filament was provided by Flashforge 3D Technology Co. Ltd. which has a uniform diameter of 1.75 mm (with tolerance ± 0.1). It has a melting point of 200°C to 220°C, and mass density of 1.210–1.430 gm/cm$^3$.

We excavated all four subterranean nests of ants in a woodland area near the Sabarmati River at the Indian Institute of Technology Gandhinagar (IITGN). Cement was mixed with water to form a very thin slurry, and the entire nest was filled with Cement slurry for extraction of casts of the chambers, shafts, and tunnels by pouring directly into the entrance until the nests were filled. After about 6-hour watering was made to harden the cement cast. The cement had been set sufficiently to be excavated after two days. The cast pieces were cleaned by washing with water, and the nest was reassembled; glue was used to cement the pieces together. The completed casts were taken into a 3D micro CT scanning (together with a suitable viewer or microdicom) to allow viewing of the cast in three dimensions. The scale in the images allowed various aspects of the casts to be measured. Measurements of chamber dimensions and areas were made from these images. MATLAB software with micro mesh to convert STF file to STL file and Ultimaker 3 extended machines for 3D printing was used. The 3D printed nature-inspired 3D architecture was dissolved with water to remove the 3D support (water-soluble wax); the water dissolved all the wax and result in the ants' 3D printed nest architecture accompanied by casting.

## 2.2. NUMERICAL SETUP

All simulations were performed in ANSYS MECHANICAL 19.2. We have performed linear structural analysis. The analysis is done under the compressive point load applied at the top of all structures considering PLA as material that was used in 3-D printing. The architectures' mechanical properties were evaluated using a compression test with a silica gel

or without silica gel under a controlled, transparent plastic jar. All the steps of mold making are shown in **Figure 1(a-f)**.

**Figure S1** represents the validation of the present model with the results of Abeykoon et al.[47]. A tensile test has been performed numerically on a PLA wire, considering the same geometry and material properties ($\rho$ = 1250 kg/m$^3$, E = 2.865 GPa, and Poisson's ratio, $\mu$ = 0.3), and boundary conditions as used in the previously published article[47]. It is observed from **Figure S1** that the present result is in very good agreement with the results of Abeykoon et al.[47].

## 3. RESULTS AND DISCUSSION

The ant mounds are excavated and scanned for the development of 3D replicas. These 3D structures are fabricated via the 3DP technique with PLA. Structural features are observed in four ant mounds structures (AM 1-4). AM1 & 2 are composed of one tapered pillar. AM1 has a thicker pillar that gradually narrows from top to middle and beyond that broadens from middle to bottom, creating an hourglass-like shape. Pillar height is smaller and thicker in AM2 than AM1, and its pillar gradually becomes narrower from top to bottom. Also, the base of AM2 is broader than AM1. In contrast, AM3 and AM4 have more than one pillar, tilted at some angles to its base. They also contain some branching features at the top of the pillar and the pillars and branches are thinner and longer than the pillar of AM1 and AM2.

To delineate the effect of structural topology and material in the complex architecture of ant mounds, we performed FEM simulation for the four geometries (AM 1-4) under different loading conditions. The simulations are performed with PLA as a material with properties such as density, $\rho$ = 1250 kg/m$^3$, and Poisson's ratio, $\mu$ = 0.3. The value of Young's modulus of elasticity obtained from the experiment given in **Table 1** has been considered for different ant mounds.

All performed simulations are mesh independent. Uniform tetrahedral mesh of with various number of elements are generated to test the convergence. **Figure S2** shows the mesh convergence test for AM1 considering a point load of 1500 N. It is observed that the variation in maximum total deformation and maximum von mises stress beyond 2511922 number of elements is relatively less, and hence it is considered for further simulation. A similar exercise has been performed for other ant mound geometries also, and finally 3666697, 1310056, and 4489067 number of elements are considered as final mesh for AM2, AM3, and AM4 respectively.

**Figure 2(a)** shows the variation of maximum total deformation and maximum Von Mises stress under varying compressive load. It is observed from **Figure 2(a)** that the maximum Von Mises stress generated in AM3 and AM4 is higher than AM1 and AM2. The thinner and longer pillars tilted at a high angle in AM3 and AM4 result in higher localized stress whereas, in AM1 and AM2 thicker pillars make it rigid and result in less stress. The lowest deformation in AM2 can be attributed to the structural topology of AM2, which consists of a small pillar with a broad base compared to the other ant mound structures. The hourglass-like shape of the pillar of AM1 results in greater deformation due to the narrow neck in the middle as compared to AM2. On the other hand, AM3 and AM4 have more than one pillar or branches (attached to the pillar), and also pillars are thinner and longer than those of structure AM1 and AM2, which results in higher deformation.

We have correlate the deformation with structural topology, the local variation of deformation and Von Mises stress under compressive point load. The contour plots for total deformation, and Von Mises stress are given in **Figure 2(c-f)** and **(g-j)**, respectively. It is observed that the maximum deformation occurs at the top of structures, where the load has been applied for the case of AM1 and AM2. However, for AM3 and AM4, maximum stress is generated at the section from where the pillar (in AM3) or its branches (in AM4) tilts. The

difference stems from the branching topology of the structure. In order to mimic the deformation of the structures under natural loading as experienced by ant mounds in the natural environment. We have also performed another set of simulations by comparing all four ant mounds when uniform pressure is applied across the whole structure. **Figure 2(b)** gives the variation of maximum total deformation and maximum Von Mises stress under varying pressure conditions. It is observed that the value of maximum total deformation is lowest for AM1 and highest for AM4. This is attributed to the fact that AM1 has a single thick pillar whereas, AM4 has two thin and long pillars which tend to deform more under pressure. AM2 and AM3 have almost the same value of maximum total deformation for all given pressure conditions. It is also observed that AM2 has the lowest stress value, followed by AM3, AM1, and AM4. The trend can be explained by the surface area upon which the pressure is applied (mean stress is inversely proportional to the applied area). **Figure 2(a)** shows the surface area value upon which pressure force is applied. It can be noted that the area of AM2 is higher than AM1 and AM3, which results in the lowest stress in AM2. However, the area of AM4 is highest, and thus accordingly, the stress in AM4 should be lowest. But, due to two long and thin pillars with branches tilted at a higher angle results in the highest stress in AM4. AM3 and AM1 having lower areas (see **Figure 2(b)**) than AM2 results in higher stress in AM1 and AM3 than AM2. Comparing AM1 and AM3, though AM1 has a higher surface area it generates higher stress than AM3. This is due to the non-uniform surface (sharp edges, hour-glass-like shape) of AM3.

Similar to the point load condition, a contour plot for uniform pressure condition has also been given for depicting the local variation of deformation and Von Mises stress. **Figure 2(k-n)** shows the contour plot for total deformation. It is observed that the deformation is maximum at thinner sections in all ant mound structures similar to the point load condition. **Figure 2(o-r)** shows the contour plot for Von Mises stress. It is observed that under uniform pressure

conditions, maximum stress is localized near the base. This is because the base area has been selected as fixed constraints and the rest area is under uniform pressure. Therefore, the maximum stress is localized at the section of applied pressure and fixed constraints.

To validate the numerical calculations, we have performed uniaxial compression of four (AM1-AM4) different ant mound structures. The load versus displacement curve has been shown in **Figure 3(a)**. Response of AM1 and AM2 under quasi-static compression in the elastic region is similar; therefore, stiffness values of AM1 and AM2 are similar (**Table 1**) to that of the numerical simulations. The load/displacement curve of AM1 attains maxima (at ~ 3 mm displacement) then drops, and the densification starts after displacement of ~5.5 mm, whereas there is no significant load drop in the case of AM2. A similar deformation/Von Mises stress trend is also observed in numerical studies (**Figure 2(a)**), where AM1 and AM2 exhibit lesser deformation and can sustain greater stress without significant deformation as compared to the other two structures (AM3 and AM4). A comparative plot of experimental and theoretical stiffness values for the four structures is shown in **Figure 3(b)**. Simulations were performed with the point load whereas, experimentally ant mound structures were tested with the uniform load on the surface of contact which causes differences in experimental and theoretical stiffness values. Both cases' trends are similar, i.e., AM2>AM1>AM3>AM4. A qualitative concordance can be drawn from the digital image of before and after deformation as seen in **Figure 3(d-g)** (experimental) and **Figure 2(c-f)** (numerical). While for AM1 and AM2, the deformed structures for both the analyses were found to be similar, AM3 and AM4 exhibit certain dissimilarities. Since these last structures (AM3 and AM4) are branched. The deformation of AM3 in the experimental case is observed in both branches, while in the simulation results, localized deformation is observed. Hence, we obtain a quantitative mismatch in the stiffness value for AM3 between experimental and simulation results. Due to the large surface area of AM4, the rotation effect in the branched structures is lesser than AM3; hence we do not observe

such quantitative discrepancy. Specific energy absorption of AM1 (253.85 J/kg) is nearly 600 times higher than AM4 (0.42 J/kg). The overall trend of the variation of energy absorption is AM1>AM2>AM3>AM4, see **Figure 3(c)**. The variation of energy absorption follows the growth pattern. In initial structures like AM1, it absorbs a large amount of energy before rupturing. As the structure grows, increasing the colony's size and topology, ants tend to segregate the nest in certain safer zones (core) to store its living supplies. Under stress conditions, another unoccupied zone deforms and absorbs energy much early than the core.

## 4. CONCLUSION

The exception mechanical robustness of the ant mount results from contribution from two different architectural components, which can be classified as primary spine (core) and secondary arms. These are gowns over a long duration. In the current work, we have studied the contribution of each of the components (primary core (AM1 and AM2) and secondary arms (AM3 and AM4)) in making structures resistant to the forces of nature. The primary spine of ant mounds appears to grow in a funnel-shaped structure from the surface level towards the bottom (AM1) and then consequently expand with an increase in surface area (as shown in AM2). This gives the typical hourglass shape to the base. These structures (as depicted in AM1 and AM2) can withstand large stress values without appreciable deformation and maintain the colony's structure. With further expansion of the surface area, the mounds appear to branch (as shown in AM3 and AM4). On the other hand, the branched structures can endure larger stress and deform in the process under a volumetric pressure application, making them sacrificial units for extreme disasters like floods and earthquakes. The 3D printing experiments and FEM simulations suggest a robust design, especially for AM1 and, in general, the possibility of constructing anthill-inspired civil buildings with a tree-trunk-like geometry.

## ACKNOWLEDGEMENT

CST acknowledge AOARD (Asian Office of Aerospace Research and Development) grant no. FA2386-19-1-4039 and Grant No. FA2386-21-1-4014. CST acknowledges Ramanujan fellowship and core research grant of SERB, India. CST acknowledge support from the Naval research board of India. CST also acknowledges the funding received from STARS project by MHRD, India.

## FUNDING

There is no funding to disclose.

## AUTHOR'S CONTRIBUTIONS

BK, AK and RSA contributed equally to this work. BK and RSA performed data curation, formal analysis and written original draft. AK and VA validated formal analysis using software and written original draft. SDN, DB, EFO and RSA carry out methodology and investigation. VP performed visualization of results. CST and CB conceptualize the idea and administrated the project. KKS, NMP, CB and CST were the supervisor and revised the paper. All authors have read and agreed to the published version of the manuscript.

## CONFLICT OF INTEREST STATEMENT

The authors declare no conflict of interest.

## REFERENCES

1. Khuong A, Gautrais J, Perna A *et al.* Stigmergic construction and topochemical information shape ant nest architecture. *Proc Natl Acad Sci U S A* 2016;**113**:1303–8.

2. Reddy LCS. Termite mound as an effective geochemical tool in mineral exploration: A study from chromite mining area, Karnataka, India. *Res J Chem Sci* 2014;**4**:85–90.

3. Singh K, Muljadi BP, Raeini AQ *et al.* The architectural design of smart ventilation and drainage systems in termite nests. *Sci Adv* 2019;**5**, DOI: 10.1126/sciadv.aat8520.

4. Chen Y, Li T, Jia Z *et al.* 3D printed hierarchical honeycombs with shape integrity under

large compressive deformations. *Mater Des* 2018;**137**:226–34.

5. Panda B, Leite M, Biswal BB *et al.* Experimental and numerical modelling of mechanical properties of 3D printed honeycomb structures. *Meas J Int Meas Confed* 2018;**116**:495–506.

6. Nian Y, Wan S, Li X *et al.* How does bio-inspired graded honeycomb filler affect energy absorption characteristics? *Thin-Walled Struct* 2019;**144**:106269.

7. Xu J, Wu Y, Wang L *et al.* Compressive properties of hollow lattice truss reinforced honeycombs (Honeytubes) by additive manufacturing: Patterning and tube alignment effects. *Mater Des* 2018;**156**:446–57.

8. Sang L, Han S, Peng X *et al.* Development of 3D-printed basalt fiber reinforced thermoplastic honeycombs with enhanced compressive mechanical properties. *Compos Part A Appl Sci Manuf* 2019;**125**:105518.

9. Kumar S, Ubaid J, Abishera R *et al.* Tunable Energy Absorption Characteristics of Architected Honeycombs Enabled via Additive Manufacturing. *ACS Appl Mater Interfaces* 2019;**11**:42549–60.

10. He Q, Feng J, Chen Y *et al.* Mechanical properties of spider-web hierarchical honeycombs subjected to out-of-plane impact loading. *J Sandw Struct Mater* 2020;**22**:771–96.

11. Fritz C, Tosello G, Fleury G *et al.* First record of the sound produced by the oldest Upper Paleolithic seashell horn. *Sci Adv* 2021;**7**, DOI: 10.1126/sciadv.abe9510.

12. Hirasawa T, Nagashima H, Kuratani S. The endoskeletal origin of the turtle carapace. *Nat Commun* 2013;**4**:2107.

13. Dimas LS, Bratzel GH, Eylon I *et al.* Tough composites inspired by mineralized natural materials: Computation, 3D printing, and testing. *Adv Funct Mater* 2013;**23**:4629–38.

14. Barthelat F, Li CM, Comi C *et al.* Mechanical properties of nacre constituents and their impact on mechanical performance. *J Mater Res* 2006;**21**:1977–86.

15. Liu X, Gu H, Ding H *et al.* Programmable Liquid Adhesion on Bio-Inspired Re-Entrant Structures. *Small* 2019;**15**:1902360.

16. Sunny S, Chen H, Malik A *et al.* Influence of residual stress and fluid–structure interaction on the impact behavior of fused filament fabrication components. *Addit Manuf* 2021;**37**:101662.

17. Minter NJ, Franks NR, Robson Brown KA. Morphogenesis of an extended phenotype: Four-dimensional ant nest architecture. *J R Soc Interface* 2012;**9**:586–95.

18. Cassill D, Tschinkel WR, Vinson SB. Nest complexity, group size and brood rearing in the fire ant, Solenopsis invicta. *Insectes Soc* 2002;**49**:158–63.

19. Tschinkel WR. The nest architecture of three species of north Florida Aphaenogaster ants. *J Insect Sci* 2011;**11**:1–30.

20. Perna A, Theraulaz G. When social behaviour is moulded in clay: On growth and form of social insect nests. Levine JD, Kronauer DJC, Dickinson MH (eds.). *J Exp Biol* 2017;**220**:83–91.

21. Verza SS, Forti LC, Lopes JFS *et al.* Nest architecture of the leaf-cutting ant Acromyrmex rugosus rugosus. *Insectes Soc* 2007;**54**:303–9.

22. Tschinkel WR. Subterranean ant nests: Trace fossils past and future? *Palaeogeogr Palaeoclimatol Palaeoecol* 2003;**192**:321–33.

23. Mikheyev AS, Tschinkel WR. Nest architecture of the ant Formica pallidefulva: Structure, costs and rules of excavation. *Insectes Soc* 2004;**51**:30–6.

24. Gautrais J, Buhl J, Valverde S *et al.* The role of colony size on tunnel branching morphogenesis in ant nests. Korb J (ed.). *PLoS One* 2014;**9**:e109436.

25. Monaenkova D, Gravish N, Rodriguez G *et al.* Behavioral and mechanical determinants of collective subsurface nest excavation. *J Exp Biol* 2015;**218**:1295–305.

26. Halley JD, Burd M, Wells P. Excavation and architecture of Argentine ant nests. *Insectes Soc* 2005;**52**:350–6.

27. Santos CM dos, Camargo R da S, Brugger M *et al.* Effect of the presence of brood and fungus on the nest architecture and digging activity of Acromyrmex subterraneus Forel (Hymenoptera, Formicidae). *Rev Bras Entomol* 2017;**61**:80–5.

28. Tschinkel WR. The nest architecture of the ant, Camponotus socius. *J Insect Sci* 2005;**5**, DOI: 10.1093/jis/5.1.9.

29. Forti LC, de Andrade APP, Camargo R da S *et al.* Discovering the giant nest architecture of grass-cutting ants, Atta capiguara (Hymenoptera, Formicidae). *Insects* 2017;**8**:39.

30. Cerquera LM, Tschinkel WR. The nest architecture of the ant odontomachus brunneus. *J Insect Sci* 2010;**10**:1–12.

31. Tiwary CS, Kishore S, Sarkar S *et al.* Morphogenesis and mechanostabilization of complex natural and 3D printed shapes. *Sci Adv* 2015;**1**:e1400052.

32. Zhu W, Li J, Leong YJ *et al.* 3D-Printed Artificial Microfish. *Adv Mater* 2015;**27**:4411–7.

33. Gao Z, Li D, Dong G *et al.* Crack path-engineered 2D octet-truss lattice with bio-inspired crack deflection. *Addit Manuf* 2020;**36**:101539.

34. Sajadi SM, Owuor PS, Schara S *et al.* Multiscale Geometric Design Principles Applied to 3D Printed Schwarzites. *Adv Mater* 2018;**30**:1704820.

35. Sajadi SM, Woellner CF, Ramesh P *et al.* 3D Printed Tubulanes as Lightweight Hypervelocity Impact Resistant Structures. *Small* 2019;**15**:1904747.

36. Ambekar RS, Mohanty I, Kishore S *et al.* Atomic Scale Structure Inspired 3D-Printed Porous Structures with Tunable Mechanical Response. *Adv Eng Mater* 2021:2001428.

37. Ambekar RS, Oliveira EF, Kushwaha B *et al.* Flexure resistant 3D printed zeolite-inspired structures. *Addit Manuf* 2021;**47**:102297.

38. Kushwaha B, Dwivedi K, Ambekar RS *et al.* Mechanical and Acoustic Behavior of 3D Printed Hierarchical Mathematical Fractal Menger Sponge. *Adv Eng Mater* 2021:2001471.

39. Sajadi SM, Owuor PS, Vajtai R *et al.* Boxception: Impact Resistance Structure Using 3D Printing. *Adv Eng Mater* 2019;**21**:1900167.

40. Ambekar RS, Kushwaha B, Sharma P *et al.* Topologically engineered 3D printed architectures with superior mechanical strength. *Mater Today* 2021;**48**:72–94.

41. Liu J, Gaynor AT, Chen S *et al.* Current and future trends in topology optimization for additive manufacturing. *Struct Multidiscip Optim* 2018;**57**:2457–83.

42. Kazakis G, Kanellopoulos I, Sotiropoulos S *et al.* Topology optimization aided structural design: Interpretation, computational aspects and 3D printing. *Heliyon* 2017;**3**:e00431.

43. Zolfagharian A, Denk M, Bodaghi M *et al.* Topology-Optimized 4D Printing of a Soft Actuator. *Acta Mech Solida Sin* 2020;**33**:418–30.

44. Zolfagharian A, Denk M, Kouzani AZ *et al.* Effects of Topology Optimization in Multimaterial 3D Bioprinting of Soft Actuators. *Int J Bioprinting* 2020;**6**, DOI: 10.18063/ijb.v6i2.260.

45. Shirzad M, Zolfagharian A, Matbouei A *et al.* Design, evaluation, and optimization of 3D

printed truss scaffolds for bone tissue engineering. *J Mech Behav Biomed Mater* 2021;**120**:104594.

46. Meiabadi MS, Moradi M, Karamimoghadam M *et al.* Modeling the Producibility of 3D Printing in Polylactic Acid Using Artificial Neural Networks and Fused Filament Fabrication. *Polymers (Basel)* 2021;**13**:3219.

47. Abeykoon C, Sri-Amphorn P, Fernando A. Optimization of fused deposition modeling parameters for improved PLA and ABS 3D printed structures. *Int J Light Mater Manuf* 2020;**3**:284–97.

**Figure 1.** The flow path of mold making (a-f). a) Original Ant mound; b) Ant mound hole pored with cement; c) Cemented Ant Mound; d) CT scan image; e) CAD Structure; f) 3D printed structure; (g-j) Different Ant Mounds. (g) AM1; (h) AM2; (i) AM3; (j) AM4.

**Figure 2**. Numerical mechanical properties of Ant Mounds. (a) Variation of the maximum total nominal deformation and maximum Von Mises stress under compressive point load for four different ant mounds. (b) Variation of the maximum total deformation and maximum Von Mises stress under uniform pressure for four different ant mounds. (c-f) Contour plot of the total deformation under 1500 N compressive load. (g-j) Contour plot of the Von Mises stress under 1500 N compressive load for all four ant mounds. (k-n) Contour plot of the total deformation under 500 MPa uniform pressure. (o-r) Contour plot of the Von Mises stress under 500 MPa uniform pressure for all four ant mounds.

**Figure 3.** Experimental mechanical properties of Ant Mounds. (a) The plot of compressive force vs. compressive vertical displacement. (b) Comparison of experimental stiffness vs numerical stiffness of ant mound structures. (c) Specific energy absorption variation with structures. (d-g) Deformation of ant mound structures under compressive load.

**Table 1.** Mechanical Properties of Ant Mounds structures.

| Structures | Stiffness (kN/m) | Specific Energy Absorption (J/kg) | Young's modulus of elasticity (GPa) |
|---|---|---|---|
| AM1 | 1369.16 | 253.8536 | 2.15 |
| AM2 | 1534.44 | 127.8675 | 0.688 |
| AM3 | 1341.25 | 7.2301 | 1.03 |
| AM4 | 59.22 | 0.4181 | 0.04 |

## Supporting information

# Understanding the Mechanics of complex topology of the 3D printed Anthill architecture

Brijesh Kushwaha[1†], Avinash Kumar[2†], Rushikesh S. Ambekar[1†*], Vinay Arya[2], Solomon Demiss Negedu[3], Deep Bakshi[4], Emmanuel Femi Olu[3], Ravi Sastri Ayyagari[4], Varinder Pal[1], Kishor Kumar Sadasivuni[5*], Nicola M. Pugno[6*], Chirodeep Bakli[2*], Chandra S. Tiwary[1*]

[1]Department of Metallurgical and Materials Engineering, Indian Institute of Technology Kharagpur, Kharagpur 721302, India

[2]School of Energy Science & Engineering, Indian Institute of Technology Kharagpur, Kharagpur 721302, India

[3]Department of Materials Science & Engineering, Jimma Institute of Technology (JIT), Jimma 378, Ethiopia

[4]Department of Mechanical Engineering, Indian Institute of Technology, Gandhinagar 382355, India

[5]Center for Advanced Materials, Qatar University, Qatar

[6]Laboratory for Bionic, Nano, Meta, Materials & Mechanics, Department of Civil, Environmental and Mechanical Engineering, University of Trento, Via Mesiano, 77, 38123 Trento, Italy

[†] Equal contribution

*Email: rambekar@iitkgp.ac.in (RSA), kishorkumars@qu.edu.qa (KKS), nicola.pugno@unitn.it (NMP), chirodeep@iitkgp.ac.in (CB) and Chandra.tiwary@metal.iitkgp.ac.in (CST)

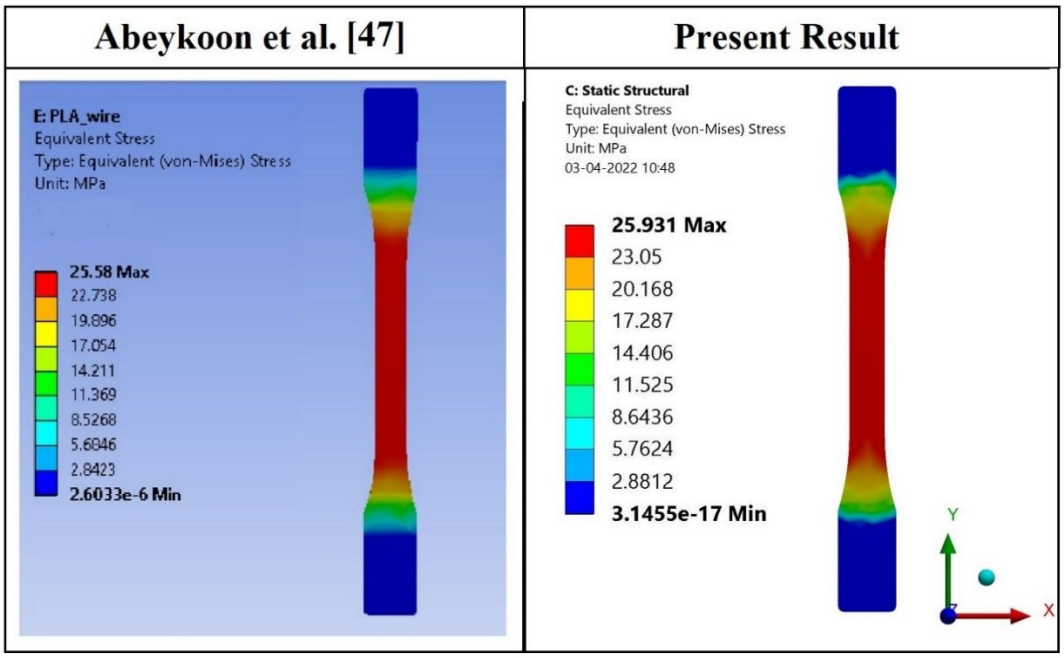


**Figure S1.** Validation of present model with results of Abeykoon et al.[47].

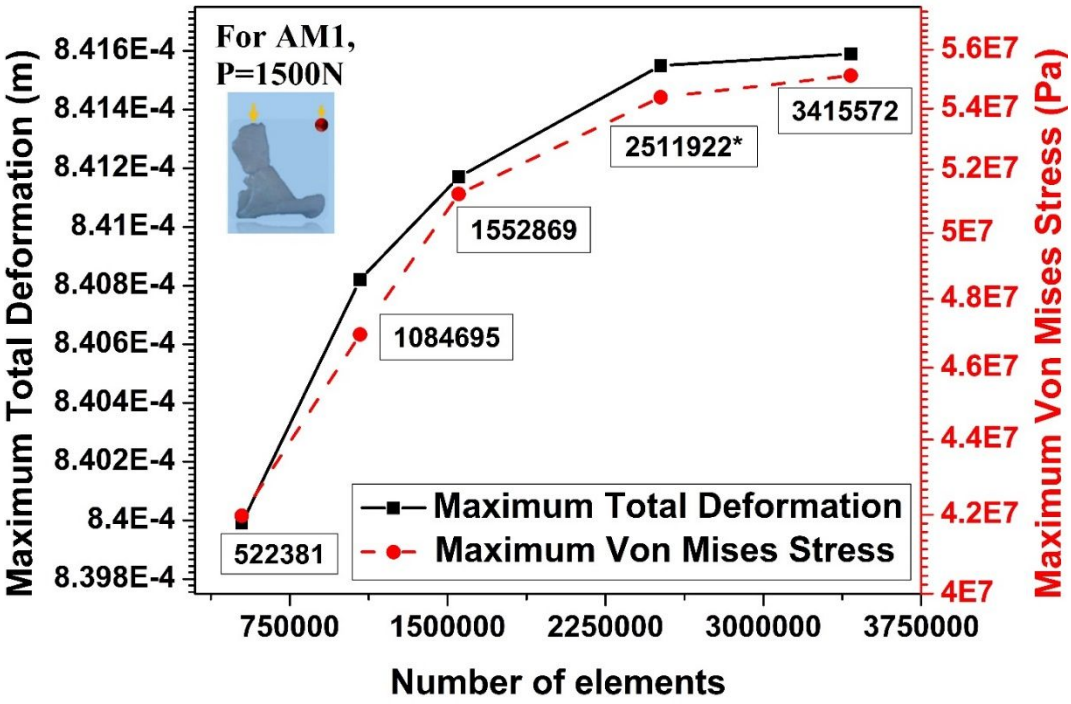


**Figure S2.** Mesh independence test for AM1 considering compressive point load of 1500 N.

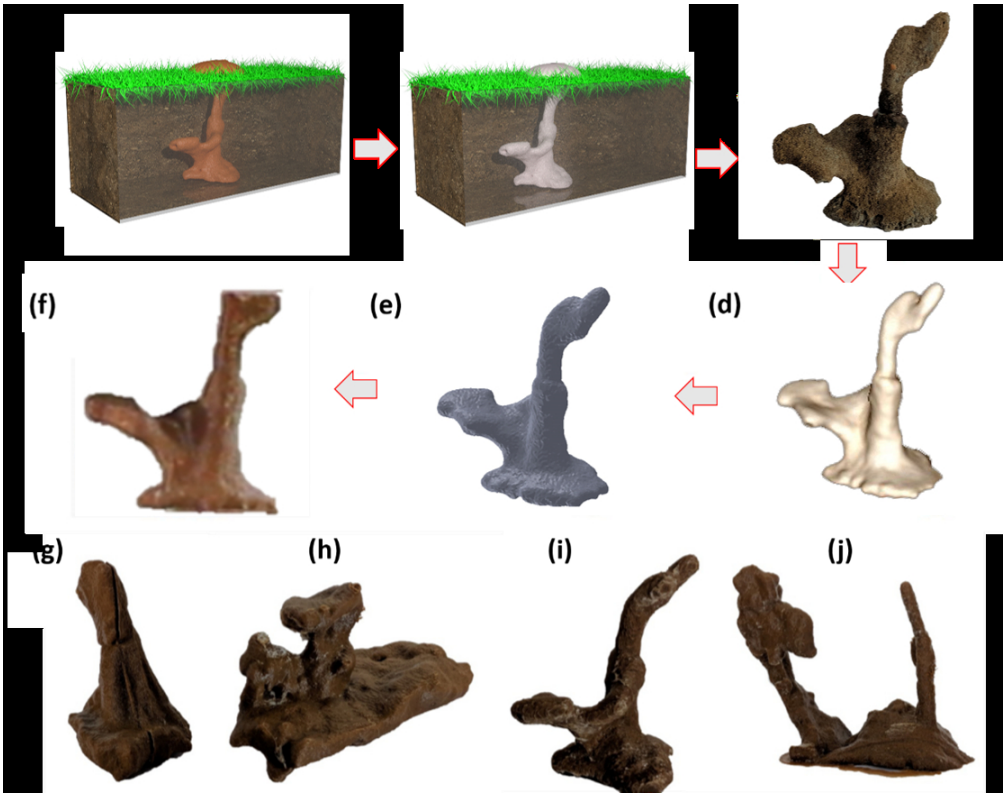


Figure 1. The flow path of mold making (a-f). a) Original Ant mound; b) Ant mound hole pored with cement; c) Cemented Ant Mound; d) CT scan image; e) CAD Structure; f) 3D printed structure; (g-j) Different Ant Mounds. (g) AM1; (h) AM2; (i) AM3; (j) AM4.

293x231mm (96 x 96 DPI)

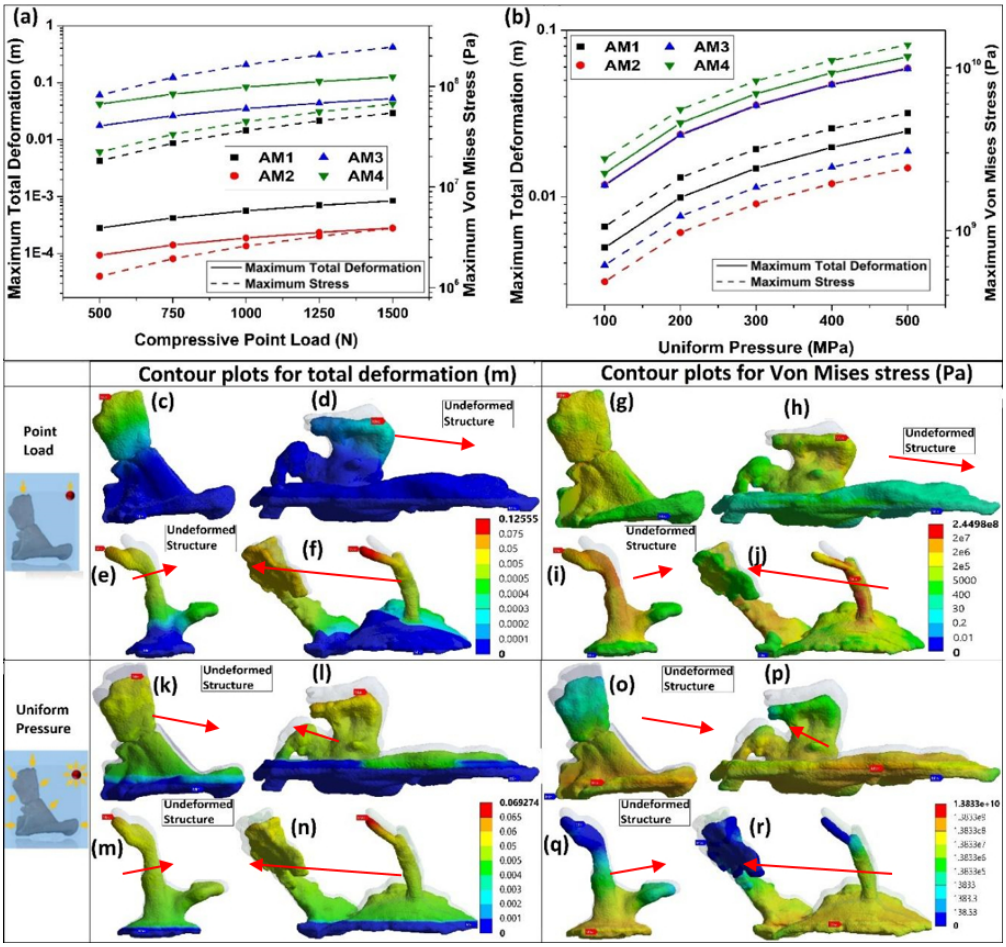


Figure 2. Numerical mechanical properties of Ant Mounds. (a) Variation of the maximum total nominal deformation and maximum Von Mises stress under compressive point load for four different ant mounds. (b) Variation of the maximum total deformation and maximum Von Mises stress under uniform pressure for four different ant mounds. (c-f) Contour plot of the total deformation under 1500 N compressive load. (g-j) Contour plot of the Von Mises stress under 1500 N compressive load for all four ant mounds. (k-n) Contour plot of the total deformation under 500 MPa uniform pressure. (o-r) Contour plot of the Von Mises stress under 500 MPa uniform pressure for all four ant mounds.

154x144mm (150 x 150 DPI)

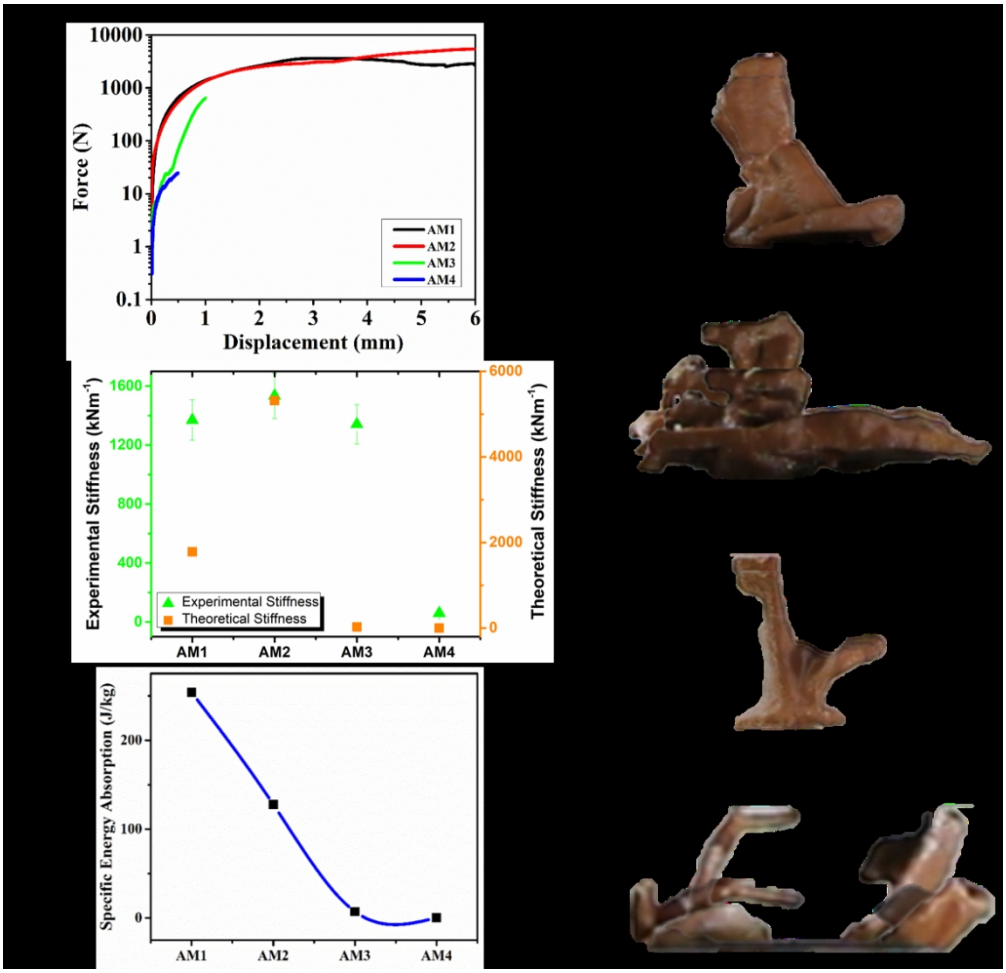


Figure 3. Experimental mechanical properties of Ant Mounds. (a) The plot of compressive force vs. compressive vertical displacement. (b) Comparison of experimental stiffness vs numerical stiffness of ant mound structures. (c) Specific energy absorption variation with structures. (d-g) Deformation of ant mound structures under compressive load.

309x298mm (96 x 96 DPI)

**Supporting information**

# Understanding the Mechanics of complex topology of the 3D printed Anthill architecture

Brijesh Kushwaha[1†], Avinash Kumar[2†], Rushikesh S. Ambekar[1†*], Vinay Arya[2], Solomon Demiss Negedu[3], Deep Bakshi[4], Emmanuel Femi Olu[3], Ravi Sastri Ayyagari[4], Varinder Pal[1], Kishor Kumar Sadasivuni[5*], Nicola M. Pugno[6*], Chirodeep Bakli[2*], Chandra S. Tiwary[1*]

[1]Department of Metallurgical and Materials Engineering, Indian Institute of Technology Kharagpur, Kharagpur 721302, India

[2]School of Energy Science & Engineering, Indian Institute of Technology Kharagpur, Kharagpur 721302, India

[3]Department of Materials Science & Engineering, Jimma Institute of Technology (JIT), Jimma 378, Ethiopia

[4]Department of Mechanical Engineering, Indian Institute of Technology, Gandhinagar 382355, India

[5]Center for Advanced Materials, Qatar University, Qatar

[6]Laboratory for Bionic, Nano, Meta, Materials & Mechanics, Department of Civil, Environmental and Mechanical Engineering, University of Trento, Via Mesiano, 77, 38123 Trento, Italy

[†] Equal contribution

*Email: rambekar@iitkgp.ac.in (RSA), kishorkumars@qu.edu.qa (KKS), nicola.pugno@unitn.it (NMP), chirodeep@iitkgp.ac.in (CB) and Chandra.tiwary@metal.iitkgp.ac.in (CST)

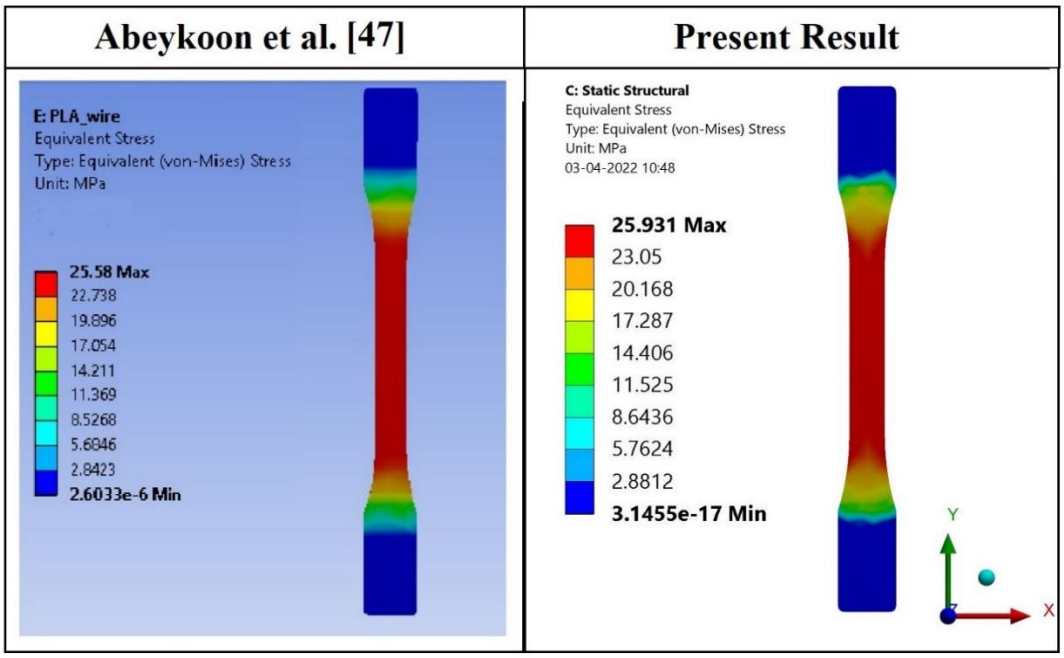


**Figure S1.** Validation of present model with results of Abeykoon et al.[47].

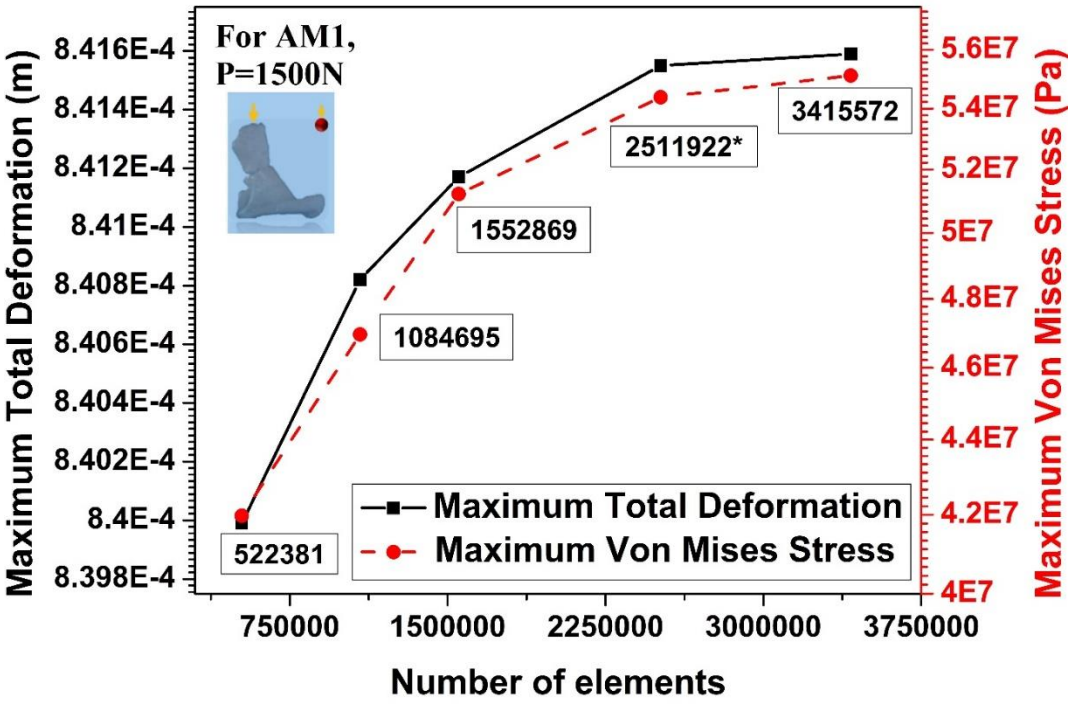


**Figure S2.** Mesh independence test for AM1 considering compressive point load of 1500 N.